ELSEVIER

Journal of Contaminant Hydrology 40 (1999) 107–136

JOURNAL OF Contaminant Hydrology

www.elsevier.com/locate/jconhyd

Numerical simulation of multiphase flow and phase partitioning in discretely fractured geologic media

K.J. Slough [a], E.A. Sudicky [a,*], P.A. Forsyth [b]

[a] *Department of Earth Sciences, University of Waterloo, Waterloo, ON, Canada N2L 3G1*
[b] *Department of Computer Science, University of Waterloo, Waterloo, ON, Canada N2L 3G1*

Received 8 December 1997; received in revised form 13 March 1999; accepted 28 April 1999

Abstract

The three-dimensional compositional model *CompFlow* has been extended to allow the simulation of the multiphase advective, dispersive and diffusive flux of non-aqueous phase liquid (NAPL) contaminants in a discrete-fracture network, allowing for phase partitioning and dynamic interactions between the fracture network and the surrounding low-permeability rock matrix. The approach used to couple fluxes between the fractures and matrix allows representation of capillary pressure differences within the fractures and matrix and makes no assumption of equilibrium hydraulic conditions between the two. The model is verified for the case of aqueous-phase solute transport by comparison with an analytical solution. An example problem is presented involving the migration of a dense non-aqueous phase liquid (DNAPL) consisting of trichloroethylene (TCE) in a single vertical fracture within a low-permeability material with significant matrix porosity. The simulation results demonstrate that matrix diffusion acts to transfer significant amounts of contaminant to the matrix in the aqueous phase. After the DNAPL source is removed, the NAPL ultimately disappears from the fracture due to partitioning of contaminant into the aqueous phase with concomitant matrix diffusion. It is shown that as the porosity of the matrix increases, the rate of migration of the TCE DNAPL front within fractures is retarded, due to dissolution and matrix diffusion. The sensitivity of DNAPL migration within the fracture to the form of the relative permeability relationship is also discussed. The model is then used to highlight the potential for deep DNAPL penetration through a vertical cross-section consisting of a shallow unconfined sand aquifer and a deeper sand aquifer separated by a layer of fractured clay. Vertical fractures through

* Corresponding author. Tel.: +1-519-888-4567, ext. 6271; fax: +1-519-746-7484; E-mail: sudicky@scisoft.uwaterloo.ca

0169-7722/99/$ - see front matter
PII: S0169-7722(99)00051-0

the clay that hydraulically connects the shallow and deep aquifers are shown to be capable of transmitting both dissolved contaminant and DNAPL to the underlying aquifer, with DNAPL travel times through the 5-m thick clay unit being on the order of days. For the scenarios examined, the DNAPL entering the lower aquifer via the fractured clay unit may completely dissolve at the aquifer–aquitard interface due to lateral groundwater flow in the lower aquifer, provided the aperture of the vertical fractures in the clay layer are less than about 50 μm; however, some DNAPL may penetrate into the lower aquifer and exist as a non-aqueous phase if the fracture apertures in the clay layer are 50 μm in size or larger. In this latter case, the presence of the DNAPL in the lower aquifer acts as a persistent source of groundwater contamination and can produce an extensive plume in the direction of groundwater flow.

Keywords: Non-aqueous phase liquids; Contaminant transport; Phase partitioning; Fractured materials; Porous materials

1. Introduction

Historically, thick deposits of lacustrine clay have been considered impermeable barriers to the downward flow of contaminants introduced accidentally at the ground surface. As a result, many industrial sites involved in the processing or storage of hazardous chemicals, particularly chlorinated organic solvents, have been situated above such clay deposits. The discovery of hydraulically active vertical fractures in clay aquitards at depths of up to 50 m has, however, caused concern for the vulnerability of deep aquifers to contamination by these dense non-aqueous phase liquids (DNAPLs). Because they are more dense and generally less viscous than water, DNAPLs composed of chlorinated organic solvents are highly mobile in the subsurface and may penetrate the fracture network within a clay aquitard and migrate downwards to contaminate drinking water sources at depth. Due to their extremely low drinking water limits, even small amounts of such solvents are capable of contaminating large volumes of water.

In a fractured low-permeability material, the entry pressure to the non wetting phase is generally lower in the fractures than the matrix. Because DNAPLs are usually non-wetting with respect to water in most geologic materials, they will preferentially enter and remain within the fracture network when a fractured low-permeability unit is encountered within the saturated zone (Kueper and McWhorter, 1991). The fracture void space in a geologic material is of the order of 10^{-3} or less of the bulk volume, while in a typical sandy aquifer, the porosity ranges from 25 to 40% (Freeze and Cherry, 1979). This means that small volumes of DNAPL may spread large distances in a fractured material relative to a similar spill volume in a typical granular aquifer. The question of the maximum vertical and lateral extents of the DNAPL source zone within a fracture network is of primary importance when assessing containment and remediation options at a fractured rock site contaminated by a DNAPL.

It is known that the diffusion of dissolved contaminants from the fractures to the matrix can retard the movement of aqueous phase solute plumes. It has also been shown by Parker et al. (1994) that the concomitant processes of dissolution and matrix diffusion

can cause the disappearance of the non-aqueous phase from fully DNAPL-saturated fractures in a high-porosity material in time frames on the order of days to years. However, it is less certain whether the processes of phase partitioning (eg. dissolution, volatilization) and matrix diffusion can reduce the mobility and maximum extent of DNAPL within a fracture network.

Previous mathematical modelling efforts addressing multiphase flow in fractured porous media have not directly addressed the issue of how aqueous-phase matrix diffusion will affect the migration rate of DNAPL fronts within a fracture network. Most previous numerical models based on the coupled two-phase flow equations (Kueper and McWhorter, 1991), as well as those based on percolation theory (Pruess and Tsang, 1990; Mendoza, 1992) which attempt to simulate the simultaneous flow of an aqueous phase and a DNAPL within a rough-walled fracture, ignored any DNAPL dissolution and matrix diffusion effects. Those models based on percolation theory which do consider DNAPL dissolution and matrix diffusion (Esposito, 1995; Banack, 1996) make the simplifying assumption that aqueous phase transport does not affect DNAPL flow; however, models such as these nevertheless provide a starting point from which to develop constitutive relationships for multiphase flow in a rough-walled fracture plane (Mendoza, 1992).

There has also been considerable work performed in developing mathematical models to simulate the transport of a dissolved solute within discrete-fracture networks within the context of single-phase groundwater flow. One of the early analytical solutions describing advective–diffusive transport of a dissolved solute in a porous medium containing a series of parallel fractures was developed by Sudicky and Frind (1982). Subsequently, numerical models were developed to investigate the effect of matrix diffusion on dissolved solutes in water-saturated fracture networks (Harrison et al., 1992; Sudicky and McLaren, 1992). Therrien and Sudicky (1996) extended these previous efforts to include solute transport in 3D fracture networks in variably saturated media. In their model, Richards' equation was used to describe flow in both the fractures and the porous matrix under the assumption that the gas phase is passive. The dissolution and transport model of VanderKwaak and Sudicky (1996) used a mixed numerical–analytical solution to study the effects of dissolution and solute transport, including matrix diffusion, on the disappearance of NAPL held within a fracture network. The DNAPL was, however, required to be at residual saturation, and thus immobile, and the distribution of the DNAPL had to be defined a priori.

Other previous numerical models have simulated the flow of DNAPL, water and gas in fractured media using a 'black-oil' approach where the effects of phase partitioning are neglected. The numerical formulation of this approach, as it pertains to fractured media, is given in Huyakorn et al. (1994), and its incorporation into a discrete-fracture model has been accomplished by Diodato (1996). Also of interest is the work of Pruess (1991) who modelled multiphase flow and transport in fractured media using the multiple interacting continua approach in the TOUGH2 simulator. This approach represents the fracture network and the porous rock matrix as separate, overlying continua which are linked by a leakage flux.

Compositional simulators (Sleep and Sykes, 1993a,b; Forsyth, 1994; Unger et al., 1995), have been shown to be robust and efficient when dealing with the complex phase

partitioning processes involved when gas, water, and a DNAPL composed of any number of components are present in porous media. Compositional models are ideally suited to multiphase problems where environmental contaminants are involved, as the model tracks the movement of each component in each phase. While appealing because of its generality, the compositional approach for modeling DNAPL migration in discrete-fracture networks embedded in a porous rock matrix has not yet been applied to the problem of multiphase flow in discretely fractured porous media.

The purpose of this paper is, firstly, to briefly describe the enhancements to a previously developed compositional numerical model, and apply this model to an investigation of DNAPL migration and phase partitioning processes in both a single vertical fracture and a fractured clay aquitard underlain by a sandy type aquifer.

2. Theory

A fully 3D, three-phase (NAPL, gas, and water) compositional model, capable of simulating the fate of DNAPLs in discretely fractured porous media, is presented. It is a direct extension of the *CompFlow* model (Unger et al., 1996), which has been previously verified against multiphase test problems involving non-fractured porous media (Panday et al., 1995). For ease of exposition and because the examples presented here involve two-phase (NAPL and water) flow, the component conservation equations for only water and contaminant are given below.

2.1. Governing equations

The equations considered in the model represent the conservation of moles for each component, ρ, which are water (w), and m contaminants ($c_1 \ldots c_m$). The two phases, l, which can exist are the non-aqueous phase (n), the aqueous phase (q). The governing equations, which are equivalent to those for multiphase flow and transport in porous media, are assumed to hold for either a discrete 2D fracture plane or a 3D porous matrix block. However, the physical properties and constitutive relations for each zone will, in general, be different. The linking between the discrete fracture and matrix equations will be discussed in Section 2.3. Assuming equilibrium partitioning of components between phases and isothermal conditions, the non-linear advective dispersive conservation equations for each component ρ are

Contaminant m conservation:

$$\frac{\partial}{\partial t}\left[\phi\left(S_q M_q X_{c_m q} + S_n M_n X_{c_m n}\right) + \rho_b K_d M_q X_{c_m q}\right] = -\Gamma\left(M_q X_{c_m q} V_q\right) - \Gamma\left(M_n X_{c_m n} V_n\right) + \Gamma\left(\phi S_q \mathbf{D}_{c_m q} M_q \Gamma X_{c_m q}\right) + \Gamma\left(\phi S_n \mathbf{D}_{c_m n} M_n \Gamma X_{c_m n}\right) + q_{c_m} \quad (1)$$

Water conservation:

$$\frac{\partial}{\partial t}\left[\phi\left(S_q M_q X_{wq}\right)\right.$$

where the Darcy flux of

$$V_l = -\mathbf{K}\frac{k_{rl}}{\mu_l}\left(\nabla P_l\right.$$

The reader should re
the text.

The constraints amo
of the dispersion tenso
have been previously p

2.2. Multiphase flow w

The surfaces of a na
in space. When multipl
will tend to occupy the
will tend to occupy the
fracture may depend c
occupied by the phase
rock fractures, Persoff
regions of narrow aper
controlled the single-p
non-wetting phase ov
Experiments involving
of flow within the frac
at different points with

When modeling mu
incorporate the effects
previously used approa
porous media, and to c
ity und phase saturat
(Kwicklis and Healy,

Relative permeabil
been investigated in
within a massive do
capillary pressure cur
Corey porous mediun
phase interference eff
phases summing to le

Water conservation:

$$\frac{\partial}{\partial t}\left[\phi\left(S_q M_q X_{wq}\right)\right] = -\nabla\left(M_q X_{wq} V_q\right) + \nabla\left(\phi S_q \mathbf{D}_{wq} M_q \nabla X_{wq}\right) \tag{2}$$

where the Darcy flux of each phase is given by (l = q,n):

$$V_l = -\mathbf{K}\frac{k_{rl}}{\mu_l}\left(\nabla P_l - \rho_l g \nabla D\right). \tag{3}$$

The reader should refer to Section 7 for the definition of any parameter not given in the text.

The constraints among the saturation, mole fraction and pressure variables, the form of the dispersion tensor, tortuosity expression and equilibrium partitioning coefficients have been previously presented (Unger et al., 1995, 1996) and are not repeated here.

2.2. Multiphase flow within a rough-walled fracture

The surfaces of a natural fracture are rough, with the fracture aperture being variable in space. When multiple fluid phases are present within a fracture, the non-wetting phase will tend to occupy the larger aperture regions of the fracture, while the wetting phase will tend to occupy the smaller aperture regions. The mobility of each phase within the fracture may depend on the degree of connection between the regions of the fracture occupied by the phase. In laboratory measurements of gas and liquid flow in natural rock fractures, Persoff and Pruess (1995) found that under certain conditions, small regions of narrow aperture located between larger regions of wider aperture effectively controlled the single-phase hydraulic aperture of the fracture, and the flow rate of the non-wetting phase over a wide range of phase saturations during two-phase flow. Experiments involving two-phase flow within fracture replicas have shown channeling of flow within the fracture and fluid velocities varying over several orders of magnitude at different points within the fracture Brown et al. (1998).

When modeling multiphase flow in a network of discrete fractures, it is desirable to incorporate the effects of these microscale processes at the macroscale of the model. A previously used approach has been to conceptualize the fracture as a 2D, heterogeneous porous media, and to define constitutive relationships between phase-relative permeability and phase saturation, as well as between phase pressure and phase saturation (Kwicklis and Healy, 1993; Therrien and Sudicky, 1996).

Relative permeability and capillary pressure relationships in a single fracture have been investigated in laboratory studies. In an experiment involving a single fracture within a massive dolomitic limestone, Reitsma and Kueper (1994) found that the capillary pressure curves measured for the fracture were well-represented by a Brooks-Corey porous medium capillary pressure function. Persoff and Pruess (1995) observed phase interference effects with relative permeabilities of the wetting and non-wetting phases summing to less than one at intermediate phase saturations.

A more theoretical approach to investigating relative permeability and capillary pressure functions in a single fracture has been to use microscale numerical models of small fracture volumes, with surface areas typically on the order of a few tens of centimeters. The fracture volumes are discretized into pore-sized segments in which the fracture walls are assumed to be smooth and parallel. Each segment is assigned a constant aperture, with the aperture distribution of the fracture generally based on statistics determined from measurements of natural fracture surfaces. Such measurements have provided experimental evidence that fracture aperture distributions may be represented by mathematical probability functions such as the log-normal distribution, and that fracture aperture is spatially correlated on the scale of a few centimeters (Gale, 1987; Brown, 1995; Hakami and Larsson, 1996).

In these microscale numerical models, each fracture segment is assumed to be occupied by only one of the wetting and non-wetting phases, with the phase occupancy governed by the local capillary pressure of the segment. Early studies, such as that by Pruess and Tsang (1990), followed a 'global accessibility' criterion, where all individual fracture segments were considered accessible to both phases. Later investigations (Mendoza, 1992; Kwicklis and Healy, 1993; Yang et al., 1995) included the effects of phase entrapment, in which disconnected clusters of fluid are not considered mobile until a continuous pathway exists from the cluster to an inflow or outflow boundary for the fluid phase in question. This approach is more suitable for situations in which the matrix surrounding the fracture is considered impermeable to the invading fluid phase, as is generally the case for a DNAPL invading a water-saturated fracture.

The work of Mendoza (1992) is particularly useful, as it examined the sensitivity of the capillary pressure and relative permeability relationships to the statistical characteristics of the fracture aperture distribution in a Monte Carlo framework. In his work, two-phase flow in a single rough-walled fracture plane was simulated using invasion percolation theory, which allowed for the entrapment of one or both fluid phases. Under various fluid accessibility scenarios, multiple realizations of the fracture aperture distribution were used to generate a range of mean capillary pressure and relative permeability curves applicable to multiphase flow within a single rough-walled fracture, and functional relationships were derived to represent them. The capillary pressure and relative permeability relationships used in this work are based on the set of simulations in which the fracture aperture was assumed to be distributed log-normally, with a variance of 1.0, a geometric mean of 27.5 μm, and an isotropic correlation structure.

As in the laboratory work of Reitsma and Kueper (1994), the capillary pressure–saturation relationships obtained by Mendoza (1992) under drainage conditions were found to be adequately represented by a Brooks–Corey type functional relationship (Brooks and Corey, 1964). The best-fit capillary pressure function, expressed in terms of areal saturations within the fracture, was (Mendoza, 1992):

$$S_{A_w}^* = \frac{S_A - S_{A_r}}{1 - S_{A_r}} = \left(\frac{\beta}{b^*}\right)^{\gamma}, \qquad (4)$$

where β is the aperture corresponding to the displacement pressure (P_d), γ is equivalent to the Brooks–Corey pore size distribution index (λ), $S_{A_w}^*$ is the effective wetting-fluid

areal saturation, and b^* is
capillary pressure for a give
this work, the effective we
the wetting phase areal s
Fractures with geometric m
applying the following sc
1992):

$$\beta = b_g \exp\left[\left(\frac{\sigma}{\sigma_0}\right)\ln($$

where b_g is the geometric
distribution, with the subs
Mendoza (1992).

The relative permeabilit
relationship. For the wet
permeability was expresse

$$k_{r_w} = S_W^{*\kappa_w},$$

where S_W^* is the wetting
of the aqueous phase wit
S_W^V) as (Mendoza, 1992)

$$S_W^* = \frac{1}{2}\mathrm{erfc}\left[\mathrm{erfc}^{-1}(

For the non-wetting p
Mendoza (1992) for drain

$$k_{r_n} = S_N^{*\kappa_{nw}}.$$

As in porous media fl
defined to represent a vol
paths. It is customary to
parallel plates, in which c
1972):

$$k = \frac{(2b)^2}{12},$$

where $2b$ is the effectiv
macrodispersion paramet
channeling and enhanced
within the fracture. Effor
macrodispersivity parame
for pore-scale variability
and Espedal, 1994; Ewin
tion of multiphase flow i

areal saturation, and b^* is the effective pore radius, subsequently used to calculate the capillary pressure for a given saturation and fluid interfacial tension. For the purposes of this work, the effective wetting-phase areal saturation was assumed to be equivalent to the wetting phase areal saturation (S_A), with a residual saturation (S_{A_r}) of zero. Fractures with geometric mean apertures other than 27.5 μm could be accommodated by applying the following scaling relationship to calculate the β parameter (Mendoza, 1992):

$$\beta = b_g \exp\left[\left(\frac{\sigma}{\sigma_0}\right)\ln(\beta_0/b_{g0})\right], \tag{5}$$

where b_g is the geometric mean aperture, and σ^2 is the variance of the log-aperture distribution, with the subscript 0 indicating the original parameter values taken from Mendoza (1992).

The relative permeability curves were found to be best represented by a simple power relationship. For the wetting-phase (water), under drainage conditions, the relative permeability was expressed as:

$$k_{r_w} = S_W^{\Delta n_w}, \tag{6}$$

where S_W^{Δ} is the wetting phase saturation expressed in areal terms. The areal saturation of the aqueous phase within the fracture was derived from the volumetric saturation (S_W^{V}) as (Mendoza, 1992):

$$S_W^{\Delta} = \frac{1}{2}\operatorname{erfc}\left[\operatorname{erfc}^{-1}(2S_W^{V}) - (1 - S_W^{V})\frac{\sigma}{\sqrt{2}}\right]. \tag{7}$$

For the non-wetting phase (DNAPL), the relative permeability was expressed by Mendoza (1992) for drainage conditions as:

$$k_{r_N} = S_N^{V\,n_N}. \tag{8}$$

As in porous media flow, the intrinsic permeability tensor of the fracture must be defined to represent a volume-averaged value of the permeability of the individual flow paths. It is customary to assume a simplified representation of the fracture as smooth, parallel plates, in which case the intrinsic permeability of the fracture is given by (Bear, 1972):

$$k = \frac{(2b)^2}{12}, \tag{9}$$

where $2b$ is the effective hydraulic aperture of the fracture. For single-phase flow, a macrodispersion parameter is also normally defined to account for the possible flow channeling and enhanced mixing of dissolved species transported in the aqueous phase within the fracture. Efforts have been made to examine the validity of defining similar macrodispersivity parameters for multiphase flow situations in porous media to account for pore-scale variability in flow velocities and the resulting fingering observed (Langlo and Espedal, 1994; Ewing, 1997). This concept is potentially applicable to the description of multiphase flow in natural fractures as well as porous media, although it has not

been applied in this work. Further effort is required to arrive at a mathematical description of the effects of channelization during multiphase flow within rough-walled fractures.

Mendoza (1992) calculated capillary pressure and relative permeability relationships under both drainage and imbibition conditions. It was observed that pore-scale variabilities caused the relationships to exhibit hysteretic behaviour at the local scale of a single fracture plane. For the purposes of this work, hysteresis is ignored at the local scale, but as discussed in Mantoglou and Gelhar (1987a; b), spatial variations in local scale properties, such as permeability and capillary pressure relationships, can cause hysteretic behaviour at a larger scale. Therefore, the incorporation of hysteresis in the local scale constitutive relationships may not be necessary to produce hysteresis within a larger-scale problem.

2.3. Numerical formulation

Eqs. (1)–(3) are discretized using the finite volume method, with the low-permeability matrix being represented by 3D rectangular block cells and the fractures by 2D rectangular planar cells. Further details regarding the discretization method can be found in Slough et al. (1998).

An input constraint on the fracture network in this version of *CompFlow* is that all fracture planes must be orthogonal. Each fracture finite volume is placed at the interface between two matrix blocks as shown in Fig. 1, and is assumed to fully intercept the flux between the two matrix cells.

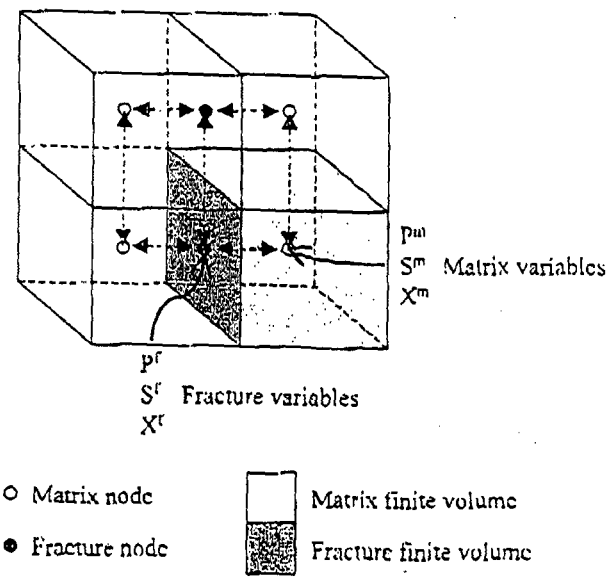

Fig. 1. Coupling of matrix and fracture finite volumes.

With this approach, coincident, and a set of addition to those at the ary differences in capilla for the inclusion of possi fracture wall. This is in modelling (Sudicky and nodes in each fracture e and a continuity of press fracture/matrix nodes.

3. Verification for aqu

A prior version of th has been previously ver work presented here is in 3D discretely fractu quently, the results of te verification of the coup analytical solution to th of parallel fractures (Su *CompFlow* model num solute concentration val

The physical system 10-m high × 2-m wide µm fracture located in

Table 1
Parameters for model verifica

Fracture	
Aperture	
Longitudinal dispersivity (α_l	
Transverse dispersivity (α_t)	
Steady-state groundwater vel	
Porosity	
Clay matrix	
Intrinsic permeability (isotrop	
(Hydraulic conductivity)	
Longitudinal dispersivity (α_l	
Horizontal transverse dispersi	
Vertical transverse dispersivit	
Porosity	
Diffusion coefficient	

With this approach, the fracture cell centre and the matrix cell centre are not coincident, and a set of primary variables is maintained at the fracture cell nodes, in addition to those at the matrix cell nodes. This dual-node approach fully incorporates any differences in capillary pressure between the fracture and the matrix, and also allows for the inclusion of possible non-equilibrium conditions due to, e.g., a 'skin effect' at the fracture wall. This is in contrast with some previous approaches to discrete fracture modelling (Sudicky and McLaren, 1992; Therrien and Sudicky, 1996), in which all nodes in each fracture element are common to those on the edges of a matrix element, and a continuity of pressure and contaminant concentration is assumed at these common fracture/matrix nodes.

3. Verification for aqueous phase transport

A prior version of the multiphase model *CompFlow* for porous media applications has been previously verified by Panday et al. (1995). To the best of our knowledge, the work presented here is the first attempt at compositional modelling of multiphase flow in 3D discretely fractured networks embedded in a porous rock matrix, and consequently, the results of test problems are unavailable in the literature to permit a complete verification of the coupled fracture/matrix multiphase flow and transport solution. An analytical solution to the problem of single-phase flow and solute transport in a system of parallel fractures (Sudicky and Frind, 1982) is used here to verify the accuracy of the *CompFlow* model numerical solution to this problem. The analytical solution provides solute concentration values at any point along the fracture or in the matrix at any time.

The physical system used in the verification and sensitivity analyses consists of a 10-m high × 2-m wide porous clay block of unit thickness with a fully penetrating 30 μm fracture located in the middle of the block. The parameters used in the verification

Table 1
Parameters for model verification

Fracture	
Aperture	30 μm
Longitudinal dispersivity (α_L)	0.01 m
Transverse dispersivity (α_T)	0.001 m
Steady-state groundwater velocity	0.53 m/day
Porosity	1.0
Clay matrix	
Intrinsic permeability (isotropic)	1.0×10^{-17} m^2
(Hydraulic conductivity)	8.0×10^{-11} m^2
Longitudinal dispersivity (α_L)	0.1 m
Horizontal transverse dispersivity (α_{T_h})	0.05 m
Vertical transverse dispersivity (α_{T_v})	0.001 m
Porosity	0.3
Diffusion coefficient	1.7×10^{-5} m^2/day

are shown in Table 1. Due to symmetry, computations were performed for only one-half of the domain. The constant pressure boundary conditions applied at the top and bottom of the domain fixed the water pressure so as to produce a steady-state downward flow of water, with a hydraulic gradient of 0.01 m/m, creating a groundwater velocity of 0.53 m/day within the fracture. The advective flux within the clay block was negligible, with velocities on the order of 10^{-7} m/day. For the verification exercise, the water entering the fracture at the upper boundary was assigned a solute concentration equal to that of TCE at its solubility limit of 1385 mg/l. No non-aqueous phase TCE existed at any time in the domain, thus permitting a direct comparison with the results of the analytical solution.

The horizontal spatial discretization used was on the order of tenths of a centimeter immediately adjacent to the fracture, and increased to a maximum of almost 20 cm at the outer edge of the domain. The vertical spatial discretization was 5 cm at the top of the fracture, and increased to a maximum of 25 cm at the bottom of the domain.

Fig. 2 shows the numerical solution of the concentration profiles along the fracture at times equal to 50 days, 1 year and 5 years, and the same concentration profiles as

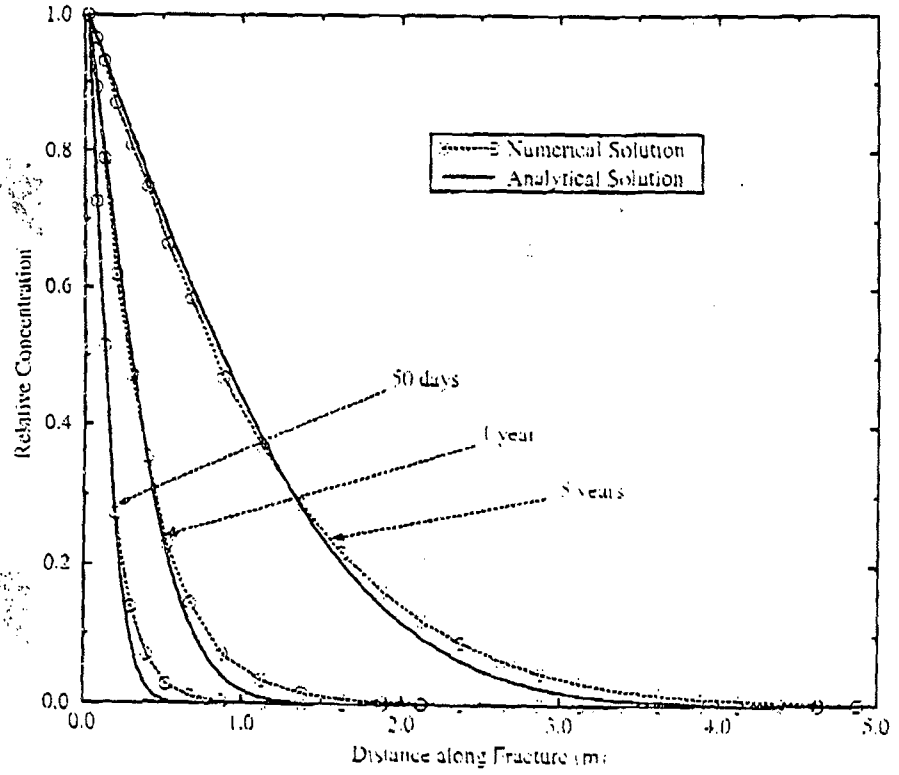

Fig. 2. Comparison of numerical and analytical solutions of concentration profile of dissolved TCE along fracture.

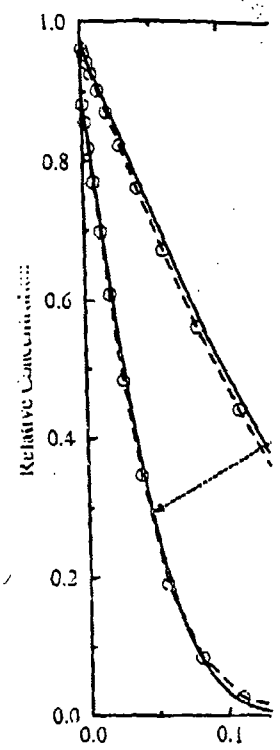

ig. 3. Comparison of numerica
.7 m below source.

predicted by the analytic
very slight amount of nu
shows the diffusion profi
depth of 0.7 m, at 1 and
Once again, clear agreem

4. DNAPL migration in

Because *CompFlow* ir
component matrix diffus
aqueous phase transport
a porous matrix.

Results will be pres
DNAPL released above

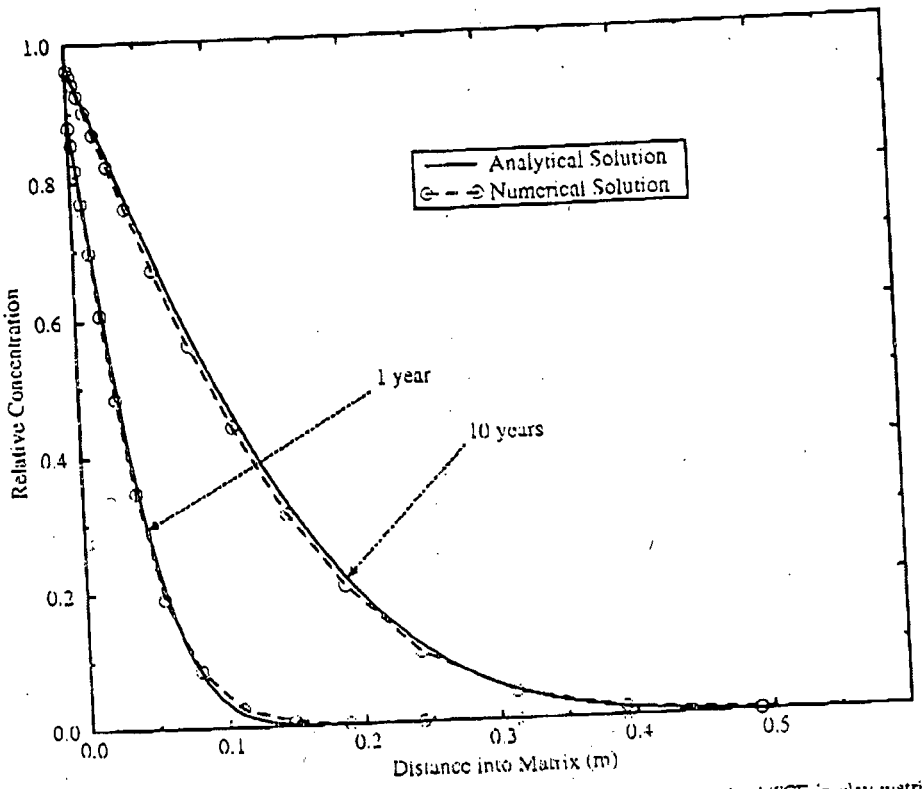

Fig. 3. Comparison of numerical and analytical solutions of diffusion profile of dissolved TCE in clay matrix 0.7 m below source.

predicted by the analytical solution. There is good agreement between the two, with a very slight amount of numerical dispersion at the leading edge of the profiles. Fig. 3 shows the diffusion profiles in the matrix, perpendicular to the plane of the fracture at a depth of 0.7 m, at 1 and 10 years for both the numerical and the analytical solutions. Once again, clear agreement exists between the numerical and analytical results.

4. DNAPL migration in a vertical fracture

Because *CompFlow* includes the processes of multiphase flow, phase partitioning and component matrix diffusion, it is ideally suited to investigate the possible influence of aqueous phase transport processes on DNAPL migration within a fracture surrounded by a porous matrix.

Results will be presented for simulations which examine the long-term fate of DNAPL released above a single vertical fracture within a clay block, and also the

sensitivity of the DNAPL migration rate within the fracture to the matrix porosity and the relative permeability–saturation relationship used within the fracture.

For these simulations, the geometry of the physical system, the properties of the geologic materials and fracture (Table 1), and the imposed hydraulic gradient were identical to those used in the verification problem. However, in this case, the top of the fracture was a release point for the chlorinated solvent, trichlorethylene (TCE). The physiochemical properties of TCE and water are given in Table 2.

The Brooks–Corey parameters used to generate the capillary pressure and relative permeability relationships within the 30-μm fracture for the two-phase system (water and a non-aqueous phase TCE) are given in Table 3. Capillary pressure relationships for the clay matrix were obtained from the work of El Kadi (1985) who compiled capillary pressure data from 175 clay samples to construct a representative capillary pressure vs. saturation curve for clay-type materials. The Brooks–Corey parameters that best represented the capillary pressure curve for clay are given in Table 3, and a capillary pressure function was calculated similar to Eq. (4), using volumetric rather than areal saturations.

Table 2
Properties of TCE and aqueous phase

Physiochemical property	Value
Free solution diffusion coefficient in water	
D^{s}_{TCE}	8.7×10^{-2} m^2/day[a]
Interfacial tension of TCE–water system	
σ_{wn}	4.4×10^{-2} N/m[a]
Liquid compressibilities	
C_q	3.0×10^{-6} kPa^{-1}[b]
C_n	4.3×10^{-7} kPa^{-1}[c]
Standard pressures	
$P^{*}_{q} = P^{*}_{n} - P^{*}_{c}$	100.0 kPa
Viscosities	
μ_w	1.43×10^{-11} kPa day[b]
μ_n	1.38×10^{-11} kPa day[b]
Molecular weights	
W_w	18.02×10^{-3} kg/mol[b]
W_{TCE}	131.5×10^{-3} kg/mol[d]
Mass density	
ρ_w	1000 kg/m^3[b]
ρ_{TCE}	1460 kg/m^3[d]
Equilibrium mole fraction in aqueous phase	1.90×10^{-4} (1385 mg/L)[d]

[a] Parker et al. (1994).
[b] Unger et al. (1996).
[c] Schwarzenbach et al. (1993).
[d] Pankow and Cherry (1996).

Table 3
Parameters used to define c
details)

	β
Fracture	33
Clay matrix	10

No relative permeab
relative permeabilitie
(8). This relationship
matrix is expected to

4.1. Long-term fate

In this problem, T
of 75 days. The relea
equal to the volume
uncontaminated wat
downwards hydrauli
implications of diffu
process known to be

As can be seen f
within the fracture, l
phase at the top of t
of TCE. After 35 d
length of the 10-m l
of the fracture. From
saturations of TCE
TCE mass entering
the lower boundary
aqueous-phase diffu

Fig. 5 shows the
Dissolved TCE can
the advective and d
only about 1% of th
was due to advecti
transport process by

After the release
phase TCE within t
boundary, until it re
entered the top of
aqueous phase in th
non-aqueous phase

Table 3
Parameters used to define capillary pressure and relative permeability relationships (see Section 2.2 for further details)

	β	γ	S_r	η_w	η_{nw}
Fracture	33.9	1.55	0.0	9.66	4.68
Clay matrix	10.11	0.34	0.19	4	4

No relative permeability relationships were available for the clay matrix, and thus, relative permeabilities were calculated using a simple power function, as in Eqs. (6) and (8). This relationship is of limited significance, as non-aqueous phase flow within the matrix is expected to be negligible.

4.1. Long-term fate of a TCE release in fractured porous media

In this problem, TCE was released at the top of the fracture, as a NAPL, for a period of 75 days. The release took place at a constant rate of 0.4 ml/day for a total of 300 ml, equal to the volume of the fracture. After 75 days, the TCE release was terminated, and uncontaminated water was allowed to flush through the fracture for 5 years, under a downwards hydraulic gradient of 0.01. This was done to examine the long-term implications of diffusion of aqueous-phase TCE from the matrix back into the fracture, a process known to be slow.

As can be seen from Fig. 4, the TCE invaded the fracture and flowed downwards within the fracture, but did not enter the clay matrix. The pressure in the non-aqueous phase at the top of the fracture was equivalent to a pool height of approximately 54 cm of TCE. After 35 days, the non-aqueous phase TCE had migrated through the entire length of the 10-m long fracture and had begun to exit through the boundary at the base of the fracture. From this point in time until the end of the TCE release (75 days), the saturations of TCE within the fracture were constant in value and equal to 0.3, with the TCE mass entering the top of the fracture equal to the total of the mass exiting across the lower boundary in both flowing phases, and the mass entering the matrix by aqueous-phase diffusion.

Fig. 5 shows the logarithm of the mole fraction of TCE in the aqueous phase. Dissolved TCE can be seen within the clay matrix. Examination of the magnitudes of the advective and diffusive mass fluxes from the fracture to the matrix indicated that only about 1% of the total flux of dissolved contaminant from the fracture to the matrix was due to advection of the aqueous phase. Thus, matrix diffusion is the dominant transport process by which dissolved TCE entered the clay matrix.

After the release of non-aqueous phase TCE was discontinued, the non-aqueous phase TCE within the fracture continued to flow downwards and exit through the lower boundary, until it reached residual saturation. At the same time, contaminant-free water entered the top of the fracture, and TCE mass partitioned from the DNAPL to the aqueous phase in the fracture. It can be seen from Fig. 4 that after less than 1 year, the non-aqueous phase was completely removed from the fracture through a combination of

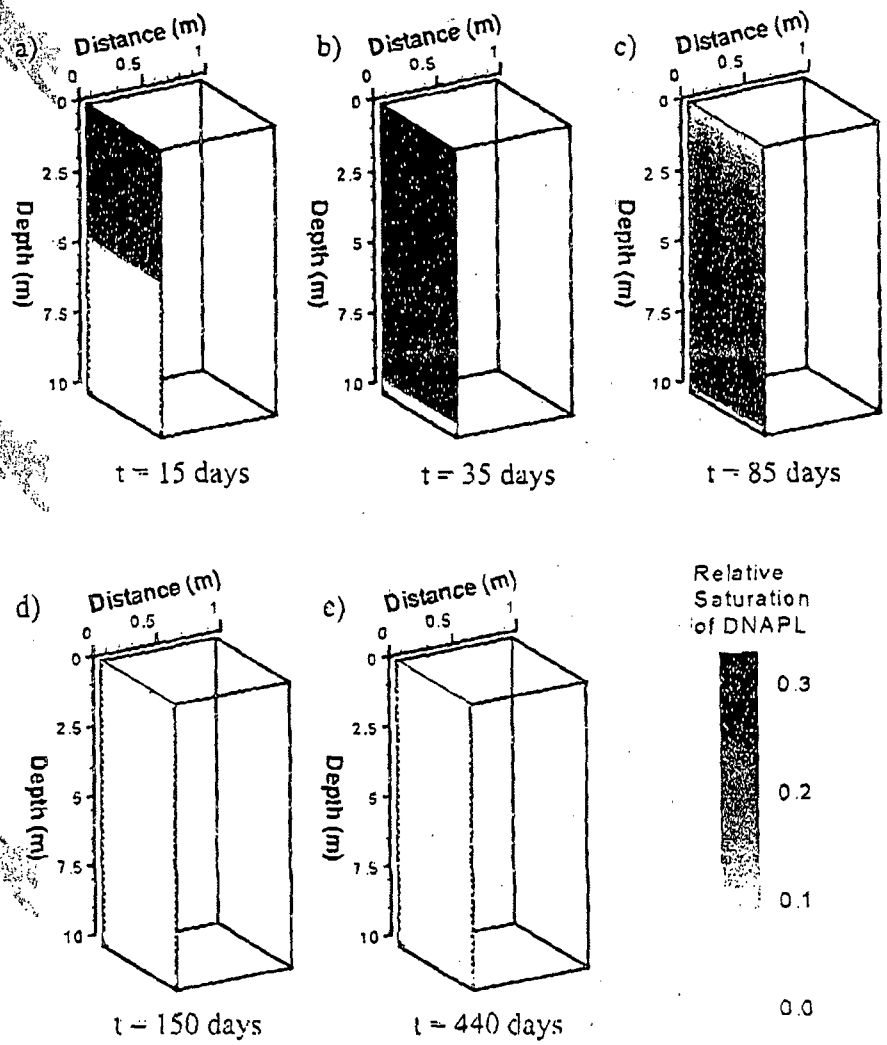

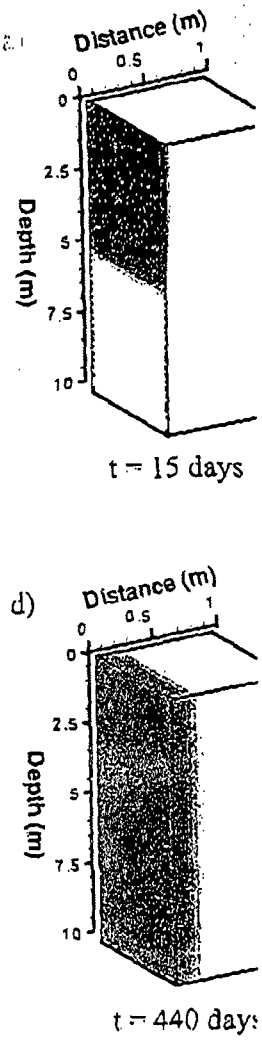

Fig. 4. The TCE saturations in fracture and matrix for 75 days of DNAPL release followed by 5 years of water flushing: (a) 15 days, (b) 35 days, (c) 85 days, (d) 150 days, (e) 440 days. (NB: leftmost vertical face of each block represents the fracture, while the remainder of the block represents the matrix.)

Fig. 5. Mole fraction of TCE i
by 5 years of water flushing: (a
vertical face of each block rep

advective flow of the non-aqueous phase through the exit boundary at the bottom of the fracture, and mass transfer to the aqueous phase.

However, by the time the DNAPL had disappeared from the fracture, approximately 10% of the TCE mass released had been transported to the matrix within the aqueous phase, primarily by matrix diffusion. This stored TCE mass continued to act as a source of contamination to the contaminant-free water entering the fracture, because the

concentration gradient at
occurs from the matrix t
time, the rate of reverse
he persistent. After allow
mass stored in the matr
leading edge of the plum

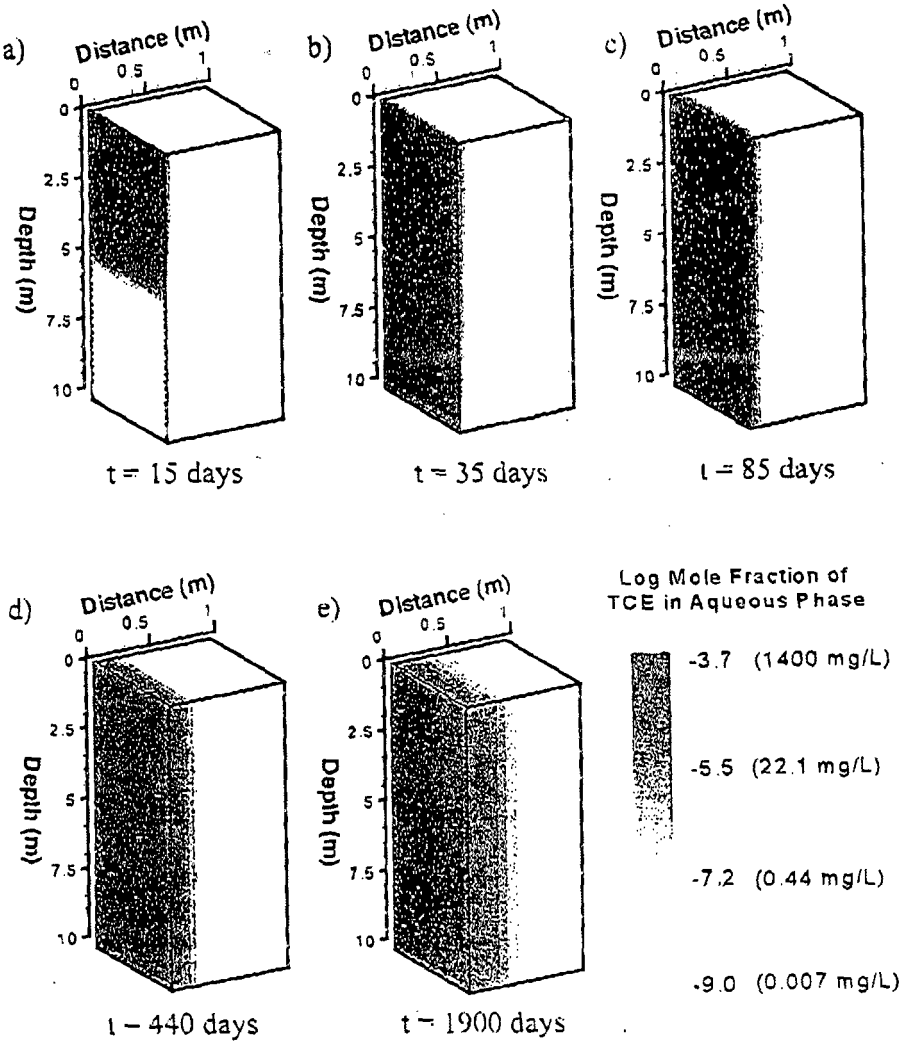

Fig. 5. Mole fraction of TCE in aqueous phase in fracture and matrix for 75 days of DNAPL release followed by 5 years of water flushing: (a) 15 days, (b) 35 days, (c) 85 days, (d) 440 days, (e) 1900 days. (NB. leftmost vertical face of each block represents the fracture, while the remainder of the block represents the matrix.)

concentration gradient at the fracture matrix interface at late time is such that diffusion occurs from the matrix to the fracture. Because the concentration gradient decreases over time, the rate of reverse diffusion will also decrease, causing the TCE contamination to be persistent. After allowing water to flush the fracture for 5 years, only 3% of the TCE mass stored in the matrix had been flushed away by water in the fracture, and the leading edge of the plume has penetrated approximately 40 cm into the clay matrix. Any

remediation scheme based solely on water flushing through the system to remove the remaining contaminant stored in the matrix will be ineffective because of the slow rate of reverse diffusion from the matrix to the fracture.

This simulation used just under 13 min of CPU time on an IBM RS/6000 series machine, rated at 32 Mflops. On a Pentium II processor, rated at 266 MHz, the same simulation required 8.3 min of CPU time. The first 75 days of the simulation, in which the DNAPL was being released, accounted for approximately 82% of the execution time. Time steps on the order of several hours were required in order that the change in phase saturation per time step at the leading edge of the DNAPL front within the fracture remained within the acceptable tolerance of 0.1. The small volume of the fracture cells exacerbated this problem. Once the DNAPL release had been terminated and the DNAPL had become immobile at residual saturation, time steps on the order of several weeks were possible.

4.2. Sensitivity of DNAPL migration rate to matrix porosity

For purposes of illustrating the relationship between the aqueous-phase diffusive flux of a dissolved solute to the matrix, the expression giving the total mass diffused into the

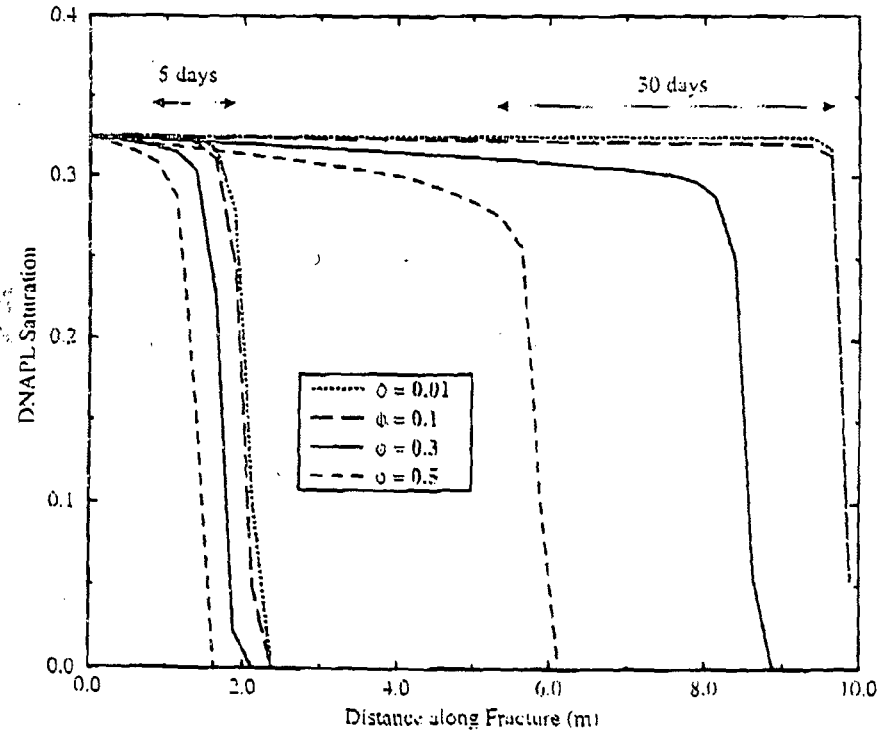

Fig. 6. Effect of matrix porosity (ϕ) on migration of DNAPL saturation front.

matrix at time t, per uni
given as (Parker, 1996):

$$M_c = \phi S_w \frac{4}{\sqrt{\pi}} \sqrt{R}$$

This analytical result a
physical parameters wh
matrix porosity (ϕ), ret
matrix tortuosity (τ). Th
coefficient. In this worl
porosity and phase satur
al., 1995).

The porosity of the
which is in the range o
porosity in the range of

Fig. 6 shows the sat
(ϕ) of 0.01, 0.1, 0.3,
release. The effect of
having reached the bot
porosity materials, whil
with a matrix porosity

4.3. Sensitivity to the re

The relative permea
functions of the phase
fracture, even under co
sensitive the DNAPL
that highly non-linear
efficiency of converge

Fig. 7 shows the se
simple test problem usi
of a different degree
exponents η_w and η_n
fracture (Eqs. (6) and (
other than the relative
presented above.

From Fig. 7, it can
a noticeable effect on
penetration of the DN
permeability function
maximum of 10 to 20
non-linear relative perm

matrix at time t, per unit area of fracture, based on a solution to Fick's Second Law is given as (Parker, 1996):

$$M_c = \phi S_w \frac{4}{\sqrt{\pi}} \sqrt{\overline{R(D^*\tau)}\, t} \tag{10}$$

This analytical result assumes 1D diffusion perpendicular to the fracture plane. The physical parameters which will control the rate of diffusive flux are seen to be the matrix porosity (ϕ), retardation factor (R), free-solution diffusion coefficient (D^*), and matrix tortuosity (τ). The latter two are often grouped together as the effective diffusion coefficient. In this work, the effective diffusion coefficient is dependent on the matrix porosity and phase saturation, through the saturation-dependent tortuosity term (Unger et al., 1995).

The porosity of the matrix material was varied from that typical of crystalline rock which is in the range of 0.1–1%, to that of a highly porous material such as clay with porosity in the range of 30–70% (Freeze and Cherry, 1979).

Fig. 6 shows the saturation profile of TCE within the fracture for matrix porosities (ϕ) of 0.01, 0.1, 0.3, and 0.5 at both 5 days and 30 days after the start of the TCE release. The effect of the matrix porosity is noticeable at 30 days, with the DNAPL having reached the bottom of the fracture for the two cases involving the low matrix porosity materials, while having penetrated only 6 m along the fracture for the material with a matrix porosity of 50%.

4.3. Sensitivity to the relative permeability function in the fracture

The relative permeability relationships, as described in Eqs. (6)–(8), are non-linear functions of the phase saturations. As they are exceedingly difficult to measure for a fracture, even under controlled laboratory conditions, it is important to determine how sensitive the DNAPL migration rate is to their precise form. Another consideration is that highly non-linear relationships in the discretized equations may decrease the efficiency of convergence in the Newton iteration.

Fig. 7 shows the saturation profiles within the fracture at a time of 30 days for a simple test problem using three sets of relative permeability curves for the fracture, each of a different degree of non-linearity. This was done by using three different sets of exponents η_w and η_n in the calculation of the relative permeability function in the fracture (Eqs. (6) and (8)), as shown in Fig. 7. The domain and basic input parameters, other than the relative permeability curves, are identical to those used in the problems presented above.

From Fig. 7, it can be seen that the form of the relative permeability relationship has a noticeable effect on the saturation of DNAPL within the fracture and the depth of penetration of the DNAPL within the fracture. The effect of the form of the relative permeability function on the efficiency of the Newton iteration was small, with a maximum of 10 to 20% reduction in the execution time for the case where the least non-linear relative permeability curves were used.

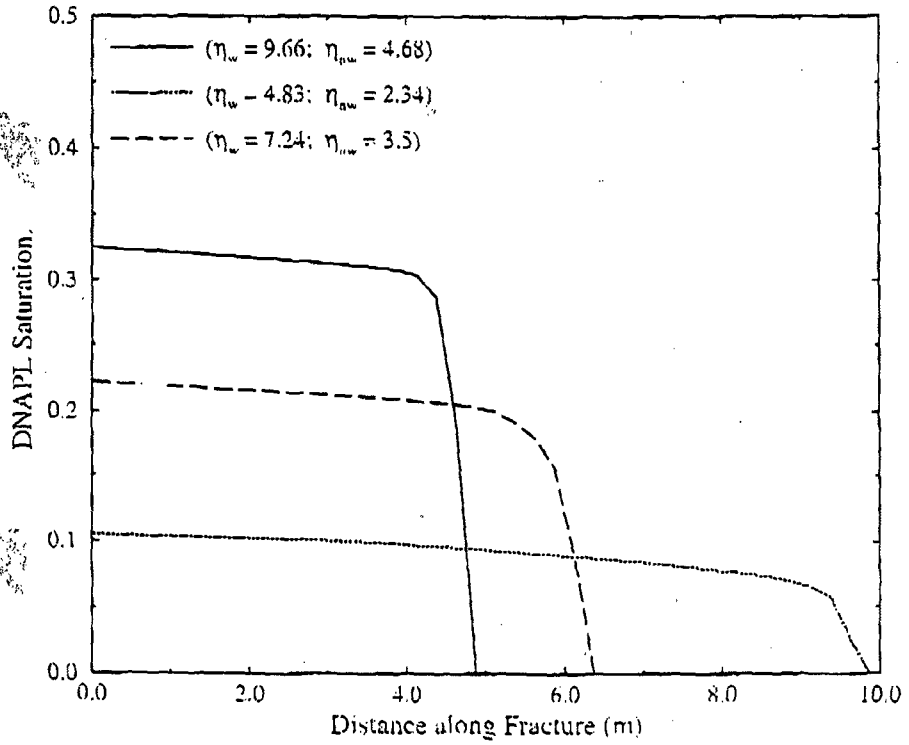

Fig. 7. Sensitivity of migration of DNAPL saturation front in a vertical fracture to form of DNAPL–water relative permeability curve (at $t = 30$ days).

These simulations show that when a large density contrast exists between the DNAPL and the aqueous phase and there is a large vertical component to flow, the rate of DNAPL migration and the relative saturation of DNAPL within a single fracture are very sensitive to the exact form of the relative permeability functions. Further simulations performed show that for the case of DNAPL migration in a horizontal fracture, the exact form of the relative permeability functions had little effect on the DNAPL migration rate.

5. DNAPL release above a fractured clay aquitard

Section 4 highlighted the effect of some of the more important parameters influencing the flow of DNAPL in a single vertical fracture which penetrates a low-permeability unit; however, it did not address the movement of immiscible fluids and the formation of aqueous-phase plumes in a complex network of fractures, nor the potential for lateral spreading of DNAPL on the top of a low-permeability unit as it builds sufficient fluid

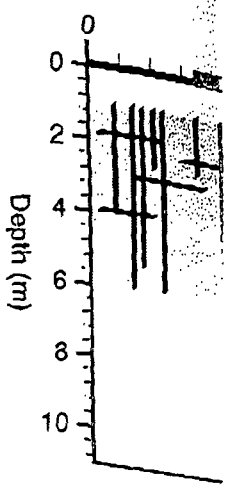

DNAPL R
Clay Aqui
Sandy Aq

Fig. 8. Pre

pressure to overcome
low-permeability unit.
Previous field stud
al., 1993) have provid

Table 4
Material properties for frac

Sand aquifers	
Intrinsic permeability (isotr	
(Hydraulic conductivity)	
Longitudinal dispersivity (a	
Horizontal transverse disper	
Vertical transverse dispersiv	
Porosity	
Clay aquitard	
Intrinsic permeability (isotr	
(Hydraulic conductivity)	
Longitudinal dispersivity (a	
Horizontal transverse disper	
Vertical transverse dispersiv	
Porosity	
Fracture aperture (2b)	

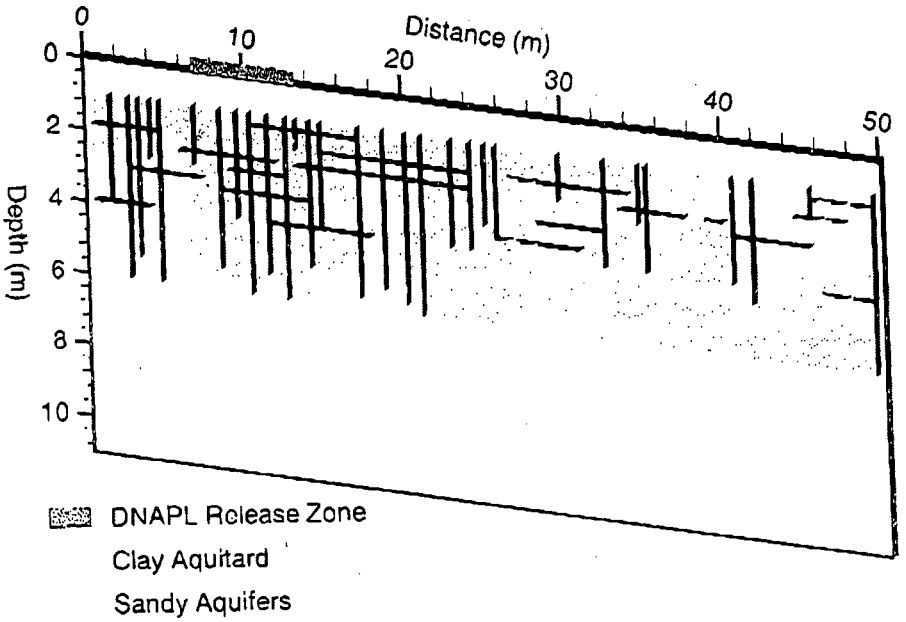

Fig. 8. Problem domain for DNAPL release above a fractured clay aquitard.

pressure to overcome the entry pressure of fractures which may intersect the top of the low-permeability unit.

Previous field studies of a natural surficial clay till near Sarnia, Ontario (McKay et al., 1993) have provided a detailed mapping of fracture spacing and apertures found in a

Table 4
Material properties for fracture network experiment

Sand aquifers	
Intrinsic permeability (isotropic)	1.0×10^{-11} m^2
(Hydraulic conductivity)	8.0×10^{-4} m/s
Longitudinal dispersivity (α_l)	0.5 m
Horizontal transverse dispersivity (α_{t_h})	0.03 m
Vertical transverse dispersivity (α_{t_v})	0.001 m
Porosity	0.3
Clay aquitard	
Intrinsic permeability (isotropic)	1.0×10^{-17} m^2
(Hydraulic conductivity)	8.0×10^{-11} m/s
Longitudinal dispersivity (α_l)	0.1 m
Horizontal transverse dispersivity (α_{t_h})	0.03 m
Vertical transverse dispersivity (α_{t_v})	0.001 m
Porosity	0.5
Fracture aperture ($2b$)	30 μm

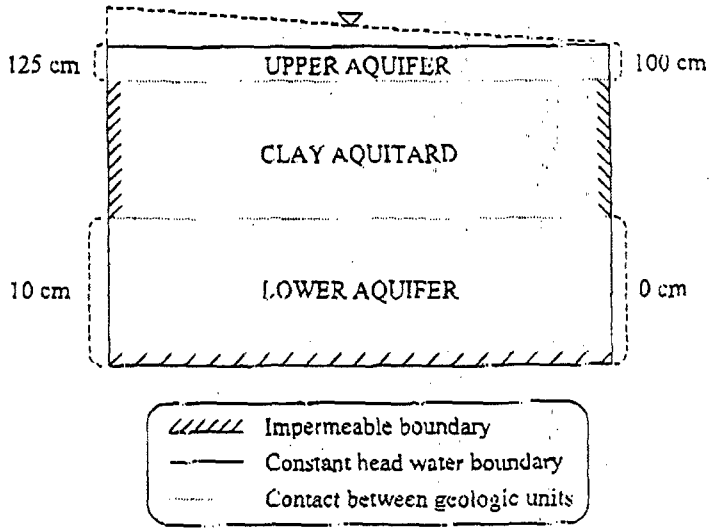

Fig. 9. Prescribed groundwater flow boundary conditions for fracture network example.

typical glacial clay deposit in southwestern Ontario. The fractures were predominantly vertical with some being horizontal in orientation, and the frequency of fracturing decreased with depth. Previous modelling studies (Harrison et al., 1992; Sudicky and McLaren, 1992) have used these field observations as a guide in designing a fracture network to examine aqueous-phase transport of a dissolved contaminant within such a fractured clay environment. In this work, a similar fracture network was designed for the purpose of simulating DNAPL migration and aqueous-phase plume development within a fractured clay aquitard.

5.1. Problem domain

The domain for the fracture network problem, shown in Fig. 8, is 50 m in length × 11 m in thickness. Although the numerical model is capable of simulating DNAPL migration in a fully 3D system, the problem addressed here is 2D with all cells being of unit thickness.

The domain consists of a 1-m thick unconfined sandy aquifer, below which is a 5-m thick, fractured clay aquitard. Below the clay aquitard is a 5-m thick sandy aquifer. The fractures are assumed to have a hydraulic aperture of 30 μm which is in the range of values estimated by McKay et al. (1993) in their field studies. Most of the vertical

Fig. 10. The DNAPL saturations for DNAPL release above a fractured clay aquitard: (a) 30 μm fracture network at 25 days, (b) 30 μm fracture network at 75 days, (c) 50 μm fracture network at 75 days.

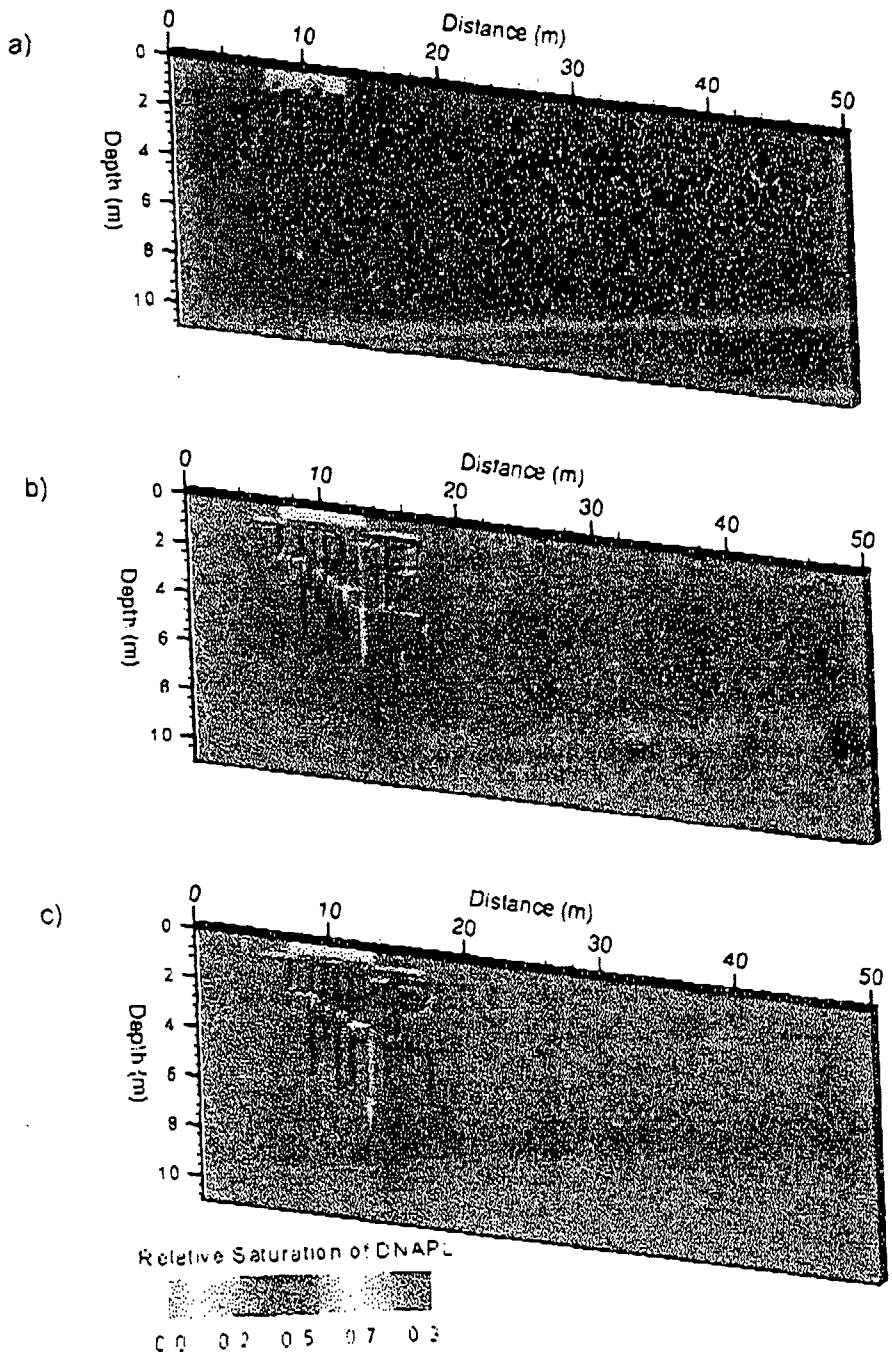

fractures terminate within the clay aquitard, but two vertical fractures, one at a horizontal distance of about 5 m, and the other at about 12 m, penetrate the aquitard completely and thus hydraulically connect the upper and lower aquifers (Fig. 8). The physical properties of the aquifers and aquitard are given in Table 4. For the purposes of these simulations, the TCE is assumed to be non-sorbing, both within the aquifer and the aquitard.

The domain is initially assumed to be fully water-saturated, with the steady-state groundwater flow regime oriented generally from left to right through the aquifers and downwards through the aquitard. The contaminant may leave any specified pressure boundary under the process of advection only. The boundary conditions are summarized in Fig. 9.

The release zone for the DNAPL was located at the upper surface of the upper aquifer between horizontal distances of 7.0 m and 13.0 m, as shown by the red area in Fig. 8. A single component DNAPL composed entirely of TCE, the properties of which are given in Table 2, was released at a rate of 6.6 l/day from this zone for 75 days.

The grid was discretized with a minimum of three matrix cells between each set of adjacent parallel fractures. The dimensions of the cells varied, with the horizontal grid block size ranging between 10 and 50 cm. In the vertical direction, the grid block size was 25 cm in the two aquifers, and between 5 and 10 cm within the fractured clay aquitard. This discretization resulted in a grid with 15,400 finite volume matrix blocks, and 1700 rectangular planar fracture cells.

5.2. Results for a release above a 30-μm fracture network

Fig. 10a and Fig. 11a show the saturation of TCE and the mole fraction of TCE in the aqueous phase, respectively, at 25 days. The non-aqueous phase TCE is seen to have migrated through the upper aquifer, and pooled on top of the lower permeability clay to a depth sufficient to overcome the entry pressure of three vertical fractures in the aquitard. Low concentrations of dissolved TCE are present in the lower aquifer at 25 days, having been transported within the fully penetrating vertical fracture at a horizontal distance of approximately 12 m. At 25 days, the concentrations of dissolved TCE are much lower in the dead-end portions of the vertical fractures as there is little advective groundwater flow in these regions, resulting in diffusion-dominated transport of the dissolved TCE.

Fig. 10b shows the DNAPL saturations at a time of 75 days. Within the aquitard, the DNAPL is seen to have collected in the dead-end portions of the vertical fractures, and in the process has caused some counter-current upward flow of water within these fractures. As the DNAPL pools in the dead-end vertical fractures and the non-aqueous phase pressure increases, it can overcome the entry pressure of connected horizontal

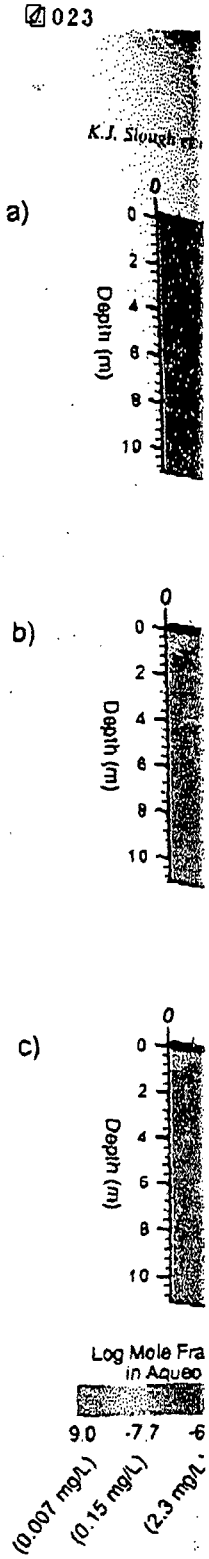

Fig. 11. Mole fraction of TCE in aqueous phase for DNAPL release above a fractured clay aquitard: (a) 30 μm fracture network at 25 days, (b) 30 μm fracture network at 75 days, (c) 50 μm fracture network at 75 days.

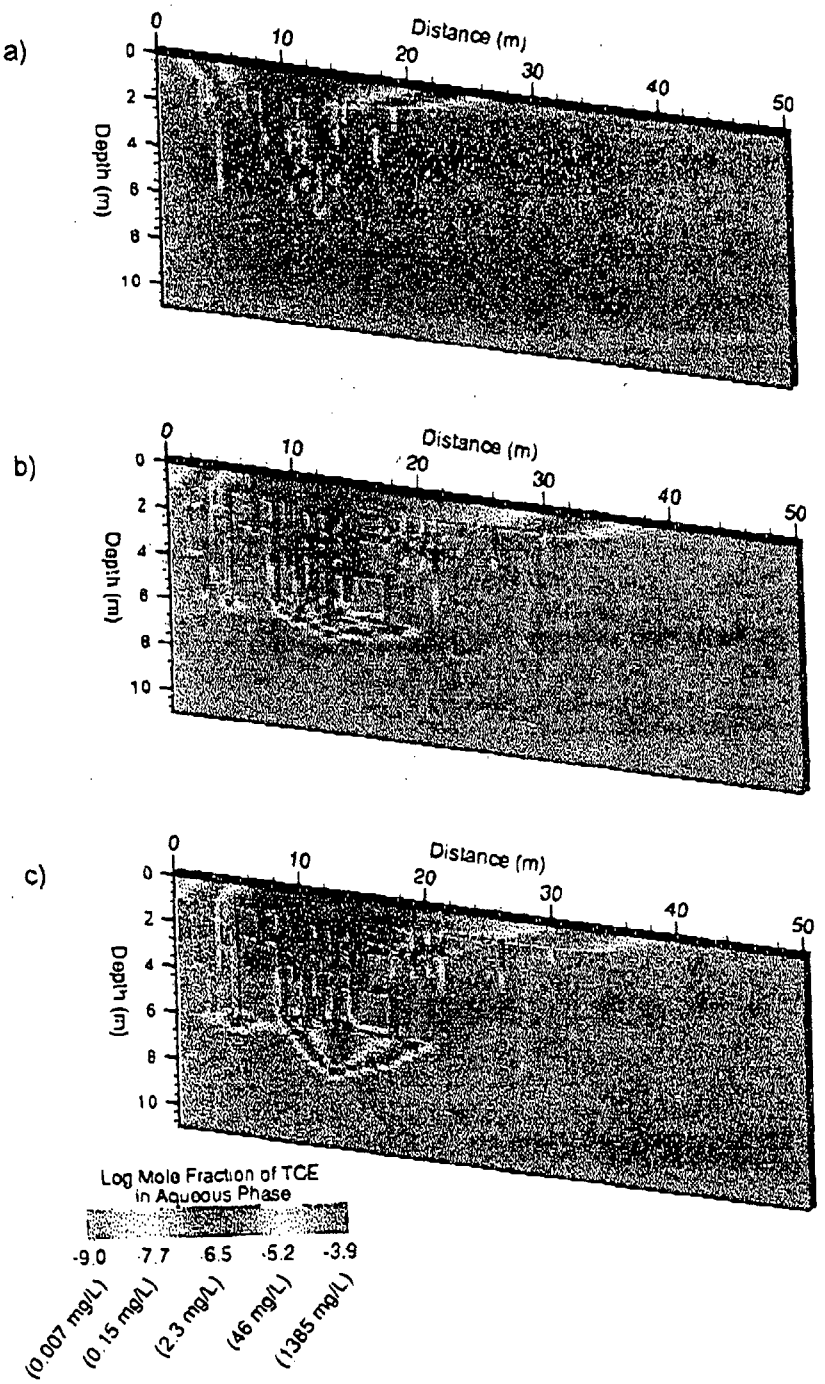
a)
b)
c)
Distance (m)
Depth (m)
0
10
20
30
40
50
2
4
6
8
10
Log Mole Fraction of TCE in Aqueous Phase
-9.0
-7.7
-6.5
-5.2
-3.9
(0.007 mg/L)
(0.15 mg/L)
(2.3 mg/L)
(46 mg/L)
(1385 mg/L)

fractures, causing the DNAPL to begin to flow in the horizontal fracture. This sudden initiation of flow within a horizontal fracture connected to a vertical one is similar to the Haines' jump seen in microscale percolation models of multiphase flow (Mendoza, 1992). Thus, the flow of the DNAPL through the fracture network is transient and erratic, and the prediction of DNAPL flow paths will be problematic.

At a time of 75 days, the extent of the DNAPL within the upper aquifer and the fracture network within the aquitard has spread laterally beyond the original boundaries of the release zone. As well, the diffusion halos of dissolved TCE in the matrix adjacent to the fractures in the clay aquitard are clearly visible in Fig. 11b.

At a time of about 40 days, the DNAPL arrived at the base of the aquitard, having migrated along the fully penetrating vertical fracture located at $x = 12$ m (results at a later time of 75 days are shown in Fig. 10b); however, no DNAPL is apparent within the lower aquifer. This is because the groundwater flowing from left to right through the lower aquifer with a Darcy flux of approximately 0.014 m/day was sufficiently rapid, and the downward flux of DNAPL through the 30-m fracture was sufficiently low such that the non-aqueous phase TCE completely dissolved as it entered the lower aquifer. This is contrary to the common conceptual model in which it is assumed that any DNAPL migrating through a fractured clay into an underlying aquifer will always form a DNAPL zone in the lower aquifer unit. For a given DNAPL, the primary factors which will determine whether the DNAPL dissolves as it enters the lower aquifer or continues to migrate downwards through it will be the mass flux of the non-aqueous phase entering the aquifer through the vertical fractures in the aquitard, and the rate of dissolution induced by the laterally flowing groundwater in the underlying aquifer. The mass flux of DNAPL entering the lower aquifer through a particular fracture will depend on a number of factors, most important of which is likely to be the fracture aperture.

5.3. Results for a release above a 50-μm fracture network

Determinations of fracture aperture in clay units are generally not made by direct measurement, but rather by calculations based on the observed fracture spacing and measured bulk conductivity of the fractured clay, resulting in some uncertainty. The sensitivity of the fate of DNAPL to the fracture aperture was examined in a simulation in which the previous DNAPL release scenario was repeated, with the network of fractures in the clay being assigned hydraulic apertures of 50 μm as opposed to 30 μm.

Fig. 10c shows the DNAPL saturations at a time of 75 days for the physical system containing the fracture network composed of 50 μm fractures. Unlike the simulation involving a 30-μm fracture network, the DNAPL which has reached the lower aquifer in this simulation has not been completely dissolved by the groundwater flowing through the lower aquifer. As a result, the DNAPL has continued to migrate downwards through the aquifer. Thus, the existence of a DNAPL source zone in a deeper aquifer overlain by a fractured clay is highly sensitive to the aperture of fractures that may penetrate the aquitard. For this 50-μm case, as the DNAPL migrates deeper into the aquifer, the overall character of the resulting solute plume, as seen in Fig. 11c, also takes on a different shape and horizontal extent as compared to the case for the 30-μm fracture case shown in Fig. 11b.

5.4. Distribution of conta

As the non-aqueous a
nant mass between the d
Fig. 12 is the total amou
TCE and the dissolved
lower aquifer vs. time for
the total mass of TCE re
time of 75 days, 97% of
more than 6 kg of TCI
vertical fracture at $x =$
upper and lower aquifer.
time, due to aqueous-pha

For comparison purp
50-μm fracture network
aquifer, in both the non-
represents about a seven

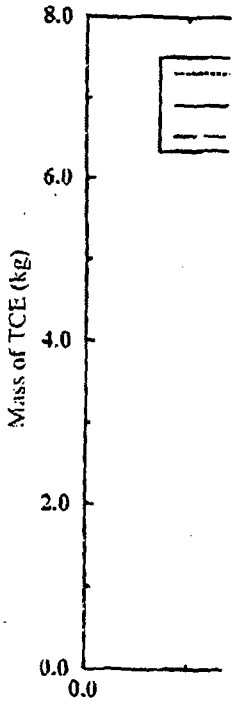

Fig. 12. Distribution of TCE

5.4. Distribution of contaminant mass over time

As the non-aqueous and aqueous phase plumes evolve, the distribution of contaminant mass between the different geologic units changes with residence time. Shown in Fig. 12 is the total amount of TCE mass, including that in both the non-aqueous phase TCE and the dissolved TCE that is stored in the fractures, the clay aquitard, and the lower aquifer vs. time for the case of the 30-m fracture network. For reference purposes, the total mass of TCE released to the domain over the 75-day period was 722 kg. At a time of 75 days, 97% of the TCE mass is located in the upper aquifer. Also at this time, more than 6 kg of TCE have entered the lower aquifer, mainly through the single vertical fracture at $x = 12$ m which is fully penetrating and hydraulically connects the upper and lower aquifer. The amount of TCE in the clay aquitard is also increasing over time, due to aqueous-phase matrix diffusion.

For comparison purposes, the distribution of TCE mass for the case involving the 50-μm fracture network is given in Fig. 13. In this case, the amount of TCE in the lower aquifer, in both the non-aqueous phase and in the aqueous phase, is about 45 kg. This represents about a sevenfold increase over that for the case of a 30-μm fracture network.

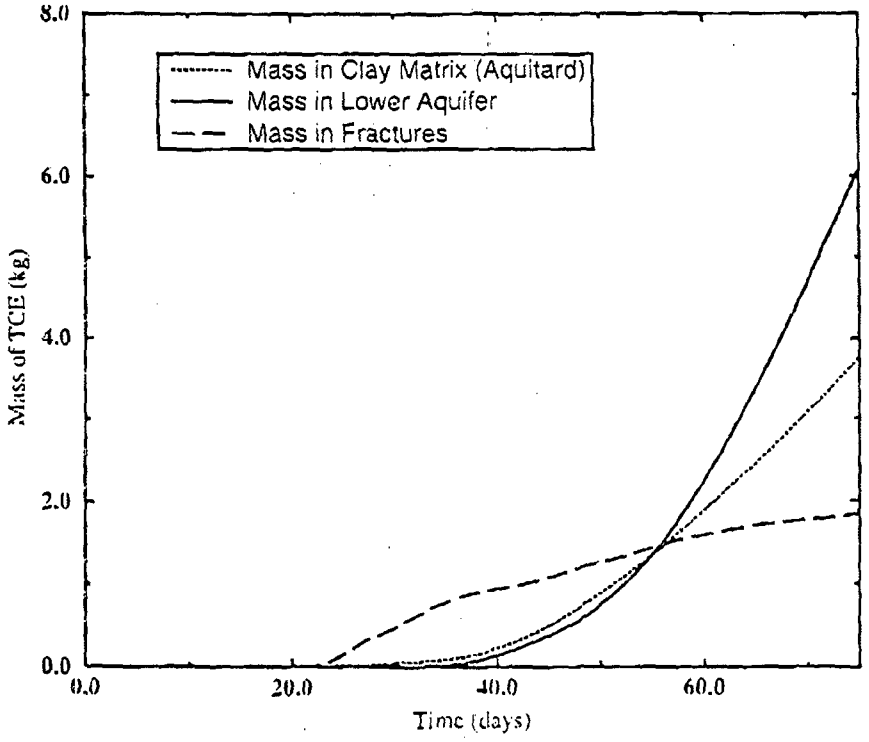

Fig. 12. Distribution of TCE Mass between geologic materials for case involving 30 μm fracture apertures.

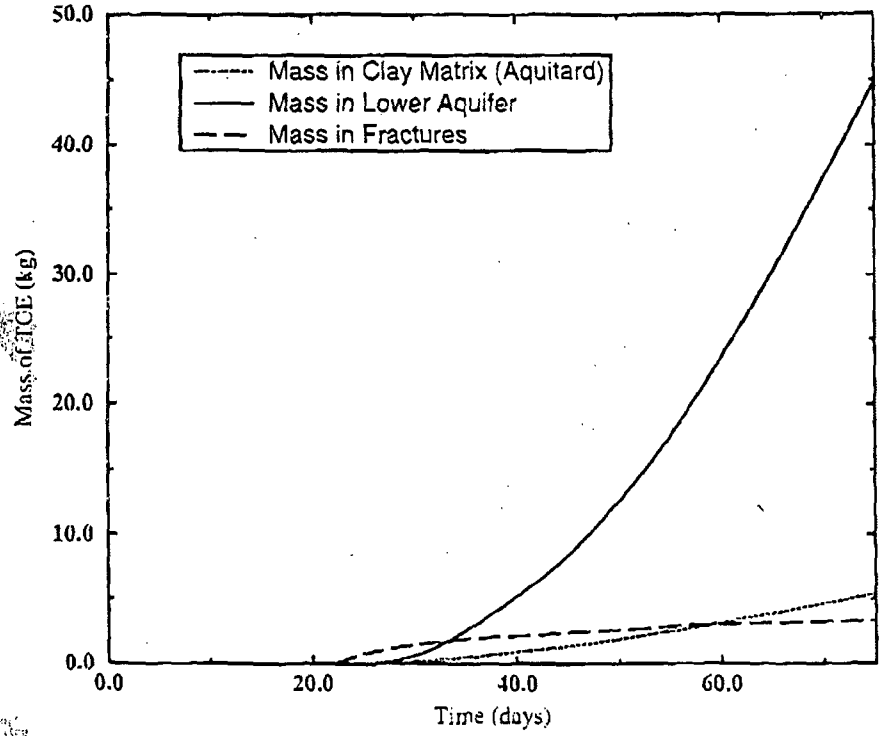

Fig. 13. Distribution of TCE mass between geologic materials for case involving 50 μm fracture apertures.

This emphasizes the sensitivity of the DNAPL flux rate through a fracture to the aperture of the fracture.

6. Conclusions

The intent of this work was to provide a means of investigating the physical process of DNAPL migration through fractured low-permeability media with significant matrix porosity. This was accomplished through an extension to the compositional model *CompFlow* to include the advective, dispersive and diffusive flux of three fluid phases (gas, water, DNAPL) within discrete fractures, and between the discrete fractures and the matrix.

An example problem involving DNAPL migration in a single vertical fracture surrounded by a low-permeability but porous matrix showed that the process of diffusion of dissolved solute to the matrix transfers significant amounts of contaminant to the matrix. Removal of contaminant from the low-permeability matrix by flushing the

fracture with uncontami
very slow.

A sensitivity analysis
the rate of DNAPL flow
were affected by diffusi
material was of high po
for numerical models t
transport rather than ass
in the aqueous phase.
strongly affects the rat
which have densities sig

A 2D simulation in
fractured clay aquitard
from DNAPLs introdu
continuous downward p
apertures are sufficientl
phase contamination to
vertical fractures at the
rate of leakage of DNA
groundwater flow in the
If this is the case, a zor
but a dissolved plume w
DNAPL due to dissoluti
aquifer underlying it is
conceptual models of th
the non-aqueous phase
other factors such as tl
thickness of the fractur
Because of the myriad
downward migration of
CompFlow model can
conceptual models.

7. Nomenclature

$2b$	fracture apertur
μ_l	viscosity of ph
ϕ	porosity [−]
ρ_b	mass density o
ρ_l	mass density of
σ^2	variance of log
D	depth [m]
D_{pl}	dispersion/diff
g	gravitational ac

fracture with uncontaminated water relies on the process of reverse diffusion, which is very slow.

A sensitivity analysis of DNAPL migration in a single vertical fracture showed that the rate of DNAPL flow and the ultimate depth of DNAPL penetration within a fracture were affected by diffusion of dissolved solute to the matrix in cases where the matrix material was of high porosity. From a numerical perspective, this emphasizes the need for numerical models to couple the effects of multiphase flow and aqueous phase transport rather than assume that the flow of the DNAPL is independent from transport in the aqueous phase. The relative permeability function assigned to a fracture also strongly affects the rate of DNAPL migration within a vertical fracture for NAPLs which have densities significantly greater than that of water.

A 2D simulation involving a scenario with a sandy aquifer situated beneath a fractured clay aquitard showed that the lower aquifer was vulnerable to contamination from DNAPLs introduced at the ground surface. It was shown that, provided a continuous downward pathway exists in the fracture network in the clay, and if fracture apertures are sufficiently large, then the possibility exists for a zone of non-aqueous phase contamination to occur within the lower aquifer; however, if the apertures of the vertical fractures at the aquifer/aquitard interface are sufficiently small such that the rate of leakage of DNAPL into the lower aquifer from the fractures is low, then lateral groundwater flow in the lower aquifer can potentially dissolve the DNAPL as it enters. If this is the case, a zone of DNAPL contamination will not form in the lower aquifer, but a dissolved plume will form and migrate laterally. The possible disappearance of the DNAPL due to dissolution at the interface between a fractured clay deposit and a sandy aquifer underlying it is an important detail which is not currently considered in previous conceptual models of the fate of DNAPLs in fractured geologic media. Whether or not the non-aqueous phase can enter and persist within the lower aquifer also depends on other factors such as the DNAPL release rate and its composition at the source, the thickness of the fractured clay layer and the diffusion/sorption properties of the clay. Because of the myriad of processes and non-linear interactions that can occur during the downward migration of DNAPL through complex multi-aquifer/aquitard systems, the *CompFlow* model can serve as a useful tool to quantitatively evaluate alternative conceptual models.

7. Nomenclature

$2b$	fracture aperture [μm]
μ_l	viscosity of phase l [Pa s]
ϕ	porosity [-]
ρ_s	mass density of solid phase [kg m^{-3}]
ρ_l	mass density of phase l [kg m^{-3}]
σ^2	variance of log-normal fracture aperture distribution
D	depth [m]
$\mathbf{D}_{pl}$	dispersion/diffusion tensor for component p in phase l [m^2 s^{-1}]
g	gravitational acceleration [m s^{-2}]

$\mathbf{K}$	absolute permeability tensor [m^2]
K_d	sorption coefficient of c_m onto solid phase [m^3 kg^{-1}]
k_{rl}	relative permeability of phase l [−]
l	phase: aqueous (q), non-aqueous (n) and gas (g)
p	component: water (w), air (a) and m contaminants ($c_{1\ldots m}$)
P_l	pressure of phase l [Pa]
q_p	source/sink term for component p [mole m^{-3} s^{-1}]
S_l	saturation of phase l [−]
V_l	Darcy flux of phase l [m s^{-1}]
W_p	molecular weight of component p [kg mol^{-1}]
X_{pl}	mole fraction of component p in phase l [−]

Acknowledgements

Funding for this work was provided by the Natural Sciences and Engineering Research Council of Canada (NSERC) in the form of a scholarship awarded to K.J. Slough, and research grants held by E.A. Sudicky and P.A. Forsyth. Funding was also obtained from the Ministry of Environment and Energy of Ontario through the Smithville Phase IV Bedrock Remediation Program, as well as the Solvents-in-Groundwater Consortium, the Waterloo Centre for Groundwater Research, and the Information Technology Research Centre. We would also like to acknowledge the expert assistance received from Dr. A.J.A. Unger while *CompFlow* was being extended to incorporate the discrete fracture network. In addition, we would like to thank the three anonymous reviewers for their comments, which have greatly improved this paper.

References

Banack, L.C., 1996. Numerical simulation of non-aqueous phase liquid dissolution in discrete rough-walled fractures. MSc Thesis, Department of Geology, University of Alberta.

Bear, J., 1972. Dynamics of Fluids in Porous Media. Elsevier, New York.

Brooks, R.H., Corey, A.T., Hydraulic properties of porous media. Hydrology Paper no. 3, Civil Engineering Dept., Colorado State University, Fort Collins, March 1964.

Brown, S., 1995. Simple mathematical model of a rough fracture. J. Geophys. Res. 100 (B4), 5941–5952.

Brown, S., Caprihan, A., Hardy, R., 1998. Experimental observation of fluid flow channels in a single fracture. J. Geophys. Res. Solid Earth 103 (3).

Diodato, D., 1996. Fractured porous media multiphase flow simulations using FracFlow 96. Abstracts from GSA Annual Meeting.

El Kadi, A.I., 1985. On estimating the hydraulic properties of soil; 1. Comparison between forms to estimate the soil water characteristic function. Adv. Water Resour. 8 (3), 136–147.

Esposito, S., 1995. Two phase flow and transport in a single fracture - porous medium system. MASc Thesis, Department of Civil Engineering, University of Waterloo.

Ewing, R.E., 1997. Aspects of upscaling in simulation of flow in porous media. Adv. Water Resour. 20 (5), 349–358.

Forsyth, P.A., 1991. Three-dimensional modelling of steam flush for DNAPL site remediation. Int. J. Numer. Methods Fluids 19, 1055–1081.

Freeze, R.A., Cherry, J.A., 1979. Groundwater. Prentice-Hall, Englewood Cliffs, NJ, 1979.

Gale, J.E., 1987. Comparison of coupled fracture deformation and fluid flow models with direct measurements

of fracture pore st
Mechanics, pp. 12
Hakami, E., Larsson,
J. Rock Mech. Mi
Harrison, B., Sudicky
clayey deposits in
Huyakorn, P.S., Pand
contamination in
Kueper, B.H., McWh
and rock. Ground
Kwicklis, E.M., Healy
fracture network.
Langlo, P., Espedal,
Water Res. 17, 29
Mantoglou, A., Gelha
Water Resour. Re
Mantoglou, A., Gelh
effective specific
1, 47–56.
McKay, L.D., Cherry
conductivity and
Mendoza, C.A., 1992
through rough-wa
Panday, S., Forsyth, I
simulation of NAI
Pankow, J.F., Cherry,
Press, OR, 1996.
Parker, B.L., 1996. I
liquids in fracture
Parker, B.L., Gillham
in fractured geolo
Persoff, P., Pruess, K
rough-walled rock
Pruess, K., TOUGH2
LBL-29400, Lawr
Pruess, K., Tsang, Y
rock fractures. W
Reitsma, S., Kueper,
rock fracture. Wa
Schwartzenbach, R.P.,
York, NY.
Sleep, B.E., Sykes, J
pounds: 1. Model
Sleep, B.E., Sykes, J
pounds: 2. Model
Slough, K.J., Forsyth
discretely fracture
Sudicky, E.A., Frind,
system of parallel
Sudicky, E.A., McLar
mass transport in
Therrien, R., Sudicky,
in discretely fractu

of fracture pore structure and stress-flow properties. Proceedings of the 28th U.S. Symposium on Rock Mechanics, pp. 1213–1222.

Hakami, E., Larsson, E., 1996. Aperture measurements and flow experiments on a single natural fracture. Int. J. Rock Mech. Miner. Sci. Geomech. Abstr. 33 (4), 395–404.

Harrison, B., Sudicky, E.A., Cherry, J.A., 1992. Numerical analysis of solute migration through fractured clayey deposits into underlying aquifers. Water Resour. Res. 28 (2), 515–526.

Huyakorn, P.S., Panday, S., Wu, Y.S., 1994. A three-dimensional multi-phase flow model for assessing NAPL contamination in porous and fractured media: 1. Formulation. J. Contam. Hydrol. 16, 109–130.

Kueper, B.H., McWhorter, D.B., 1991. The behaviour of dense, non-aqueous phase liquids in fractured clay and rock. Ground Water 29, 716–728.

Kwicklis, E.M., Healy, R.W., 1995. Numerical investigation of steady liquid water flow in a variably saturated fracture network. Water Resour. Res. 29 (12), 4091–4102.

Langlo, P., Espedal, M.S., 1994. Macrodispersion for two-phase, immiscible flow in porous media. Adv. Water Res. 17, 297–316.

Mantoglou, A., Gelhar, L.W., 1987a. Stochastic modelling of large-scale transient unsaturated flow systems. Water Resour. Res. 1, 37–46.

Mantoglou, A., Gelhar, L.W., 1987b. Capillary tension head variance, mean soil moisture content, and effective specific soil moisture capacity of transient unsaturated flow in stratified soils. Water Resour. Res. 1, 47–56.

McKay, L.D., Cherry, J.A., Gillham, R.W., 1993. Field experiments in a fractured clay till: 1. Hydraulic conductivity and fracture aperture. Resources Research 29, 1149–1162.

Mendoza, C.A., 1992. Capillary pressure and relative transmissivity relationships describing two-phase flow through rough walled fractures in geologic materials. PhD Thesis, Univ. of Waterloo, 1992.

Panday, S., Forsyth, P.A., Falta, R., Wu, Y.S., Huyakorn, P.S., 1995. Considerations for robust compositional simulation of NAPL contamination and remediation. Water Resour. Res. 31 (5), 1273–1289.

Pankow, J.F., Cherry, J.A., 1996. Dense Chlorinated Solvents and Other DNAPLs in Groundwater. Waterloo Press, OR, 1996.

Parker, B.L., 1996. Effects of molecular diffusion on the persistence of dense, immiscible phase organic liquids in fractured porous geologic media. PhD Thesis, Univ. of Waterloo.

Parker, B.L., Gillham, R.W., Cherry, J.A., 1994. Diffusive disappearance of immiscible phase organic liquids in fractured geologic media. Water 32 (5), 805–820.

Persoff, P., Pruess, K., 1995. Two-phase flow visualization and relative permeability measurement in natural rough-walled rock fractures. Water Resour. Res. 31 (5), 1175–1186.

Pruess, K., TOUGH2 — a general-purpose numerical simulator for multiphase fluid and heat flow, Rep. LBL-29400, Lawrence Berkeley Lab., September 1991.

Pruess, K., Tsang, Y.W., 1990. On two-phase relative permeability and capillary pressure of rough walled rock fractures. Water Resour. Res. 26 (9), 1915–1926.

Reitsma, S., Kueper, B.H., 1994. Laboratory measurement of capillary pressure–saturation relationships in a rock fracture. Water Resour. Res. 30 (4), 865–878.

Schwarzenbach, R.P., Gschwend, P.M., Imboden, D.M., 1993. Environmental Organic Chemistry. Wiley, New York, NY.

Sleep, B.E., Sykes, J.F., 1993a. Compositional simulation of groundwater contamination by organic compounds: 1. Model development and verification. Water Resour. Res. 29 (6), 1697–1708.

Sleep, B.E., Sykes, J.F., 1993b. Compositional simulation of groundwater contamination by organic compounds: 2. Model applications. Water Resour. Res. 29 (6), 1709–1718.

Slough, K.J., Forsyth, P.A., and Sudicky, E.A., 1998. Grid refinement for modeling multiphase flow in discretely fractured porous media. Adv. Water Res., submitted.

Sudicky, E.A., Frind, E.O., 1982. Contaminant transport in fractured porous media: analytical solutions for a system of parallel fractured. Resources Research 18, 1634–1642.

Sudicky, E.A., McLaren, R.G., 1992. The Laplace transform galerkin technique for large-scale simulation of mass transport in discretely fractured porous formations. Water Resour. Res. 28, 499–514.

Therrien, R., Sudicky, E.A., 1996. Three-dimensional analysis of variably saturated flow and solute transport in discretely fractured porous media. J. Contam. Hydrol. 23, 1–44.

Unger, A.J.A., Sudicky, E.A., Forsyth, P.A., 1995. Mechanisms controlling vacuum extraction coupled with air sparging for remediation of heterogeneous formations contaminated by dense non-aqueous phase liquids. Water Resour. Res. 31 (8), 1913–1925.

Unger, A.J.A., Forsyth, P.A., Sudicky, E.A., 1996. Variable spatial and temporal weighting schemes for use in multi-phase compositional problems. Adv. Water Resour. 19 (1).

VanderKwaak, J.E., Sudicky, E.A., 1996. Dissolution of non-aqueous phase liquids and aqueous-phase contaminant transport in discretely fractured porous media. J. Contam. Hydrol. 23, 45–68.

Yang, G., Myer, L.R., Brown, S.R., Cook, N.G.W., 1995. Microscopic analysis of macroscopic transport properties of single natural fractures using graph theory algorithms. Geophys. Res. Lett. 22, 1429–1432.